Dynamics of a self-diffusiophoretic particle in shear flow

Alexandra E. Frankel and Aditya S. Khair
Department of Chemical Engineering, Carnegie Mellon University, Pittsburgh, Pennsylvania 15213, USA
(Received 27 May 2014; published 31 July 2014)

Colloidal particles can achieve autonomous motion by a number of physicochemical mechanisms. For instance, if a spherical particle acts as a catalyst with an asymmetric surface reactivity, a molecular solute concentration gradient will develop in the surrounding fluid that can propel the particle via self-diffusiophoresis. Theoretical analyses of self-diffusiophoresis have mostly been considered in quiescent fluid, where the solute concentration is usually assumed to evolve solely via diffusion. In practical applications, however, self-propelled colloidal particles can be expected to reside in flowing fluids. Here, we examine the role of ambient flow on self-diffusiophoresis by quantifying the dynamics of a model Janus particle in a simple shear flow. The imposed flow can distort the self-generated solute concentration gradient. The extent of this distortion is quantified by a Peclet number, Pe, associated with the shear flow. Utilizing matched asymptotic analysis, we determine the concentration gradient surrounding a Janus particle in shear flow at a small, but finite, Peclet number and the resulting particle motion. For example, when the symmetry axis of the particle is aligned with the imposed flow, the Janus particle experiences an O(Pe) cross-streamline drift and an O($Pe^{3/2}$) reduction in translational velocity along the flow direction. We then analyze the in-plane trajectory of the Janus particle in shear. We find that the particle performs elliptical orbits around its initial position in the flow, which decrease in size with increasing Pe.

DOI: 10.1103/PhysRevE.90.013030 PACS number(s): 47.15.G−, 82.70.Dd

I. INTRODUCTION

Colloidal particles usually move at low Reynolds number, where viscous forces dominate fluid flow. In this regime, particle transport can be affected by imposed fields, including thermal gradients [1,2], concentration gradients [1–4], electric fields [3–5], and magnetic fields [3,4]. More recently, active, or self-propelled, particles have been explored as a method of directed colloidal particle movement [3,4,6–19,21]. One method of self-propulsion is self-diffusiophoresis, where a colloidal particle generates a local solute concentration gradient via a surface chemical reaction [3,4,6–13]. One of the most studied particle geometries is the Janus sphere [3,4,6–8,11,12], although the motion of self-diffusiophoretic rods and dimers has also been considered [3–5,9,10,13]. Janus particles can be fabricated by coating half of a polystyrene bead with platinum [4,6,11]. When suspended in a dilute solution of H_2O_2, the difference in the decomposition rate of H_2O_2 between the platinum and polystyrene faces of the particle creates a local asymmetric concentration gradient. This gradient results in a velocity slip around the particle [1], which causes the particle to move in order to remain force-free.

Much of the experimental and theoretical work on self-diffusiophoresis has considered particle motion in quiescent fluids [3,4,6–12]. A common modeling assumption made in these cases is that the effect of advection due to particle translation on the self-generated solute concentration gradient can be ignored because of the relatively large solute diffusivity and modest phoretic particle velocity. The relative importance of solute advection to diffusion is quantified by a Peclet number, Pe, where $\mathrm{Pe} \gg 1$ indicates that advection dominates and $\mathrm{Pe} \ll 1$ indicates that diffusion dominates. The Peclet number associated with particle translation equals aU/D, where a is the characteristic length of the particle, U is the phoretic particle speed, and D is the diffusion coefficient of the solute. Using values typical of Janus spheres, where $D \sim 10^{-9}\,\mathrm{m}^2/\mathrm{s}$, $a \sim 10^{-6}\,\mathrm{m}$, and $U \sim 10^{-6}\,\mathrm{m/s}$ [4,20], gives $\mathrm{Pe} \sim 10^{-3}$. Thus, it is reasonable to assume that advection plays a minor role in the instantaneous phoretic particle motion in this case, although cumulative effects at small Pe may be important [21]. Michelin and Lauga [22] have discussed cases in which Pe may not be small in their recent analysis of a self-diffusiophoretic Janus particle at finite Pe.

Several of the purported applications for self-propelled particles, however, do not occur in quiescent fluid. Such particles have been suggested as drug delivery vehicles through blood vessels [4,6,23–25]. The fluid flow through these vessels can be locally approximated as a shear flow with shear rate on the order of $10^2\ \mathrm{s}^{-1}$ [23,26,27]. Another application of self-propelled particles is transport through microfluidic channels for laboratory-on-a-chip devices [4,6,28]. This provides the motivation to predict the motion of self-propelled particles in ambient flows. Indeed, the effect of an ambient flow on active particles, including self-diffusiophoretic particles, has been explored [13–19,23], though to a far lesser degree than active particles in quiescent fluid. For example, the Brownian motion of a generic active particle in both shear flow and Poiseuille has been considered [15,19,23]. In those works, the phoretic velocity of the active particle was assumed to be independent of the ambient flow. In the particular case of self-diffusiophoresis, however, a shear flow can distort the self-generated solute concentration gradient through advection, consequently altering the instantaneous phoretic velocity of the particle. That is, the phoretic velocity is not independent of the imposed flow. For instance, Tao and Kapral analyzed the motion of a self-diffusiophoretic dimer particle located at the center of a Poiseuille flow in a square channel to determine the influence of channel size and solute-particle interaction on the phoretic velocity of the dimer [13]. They noted that solute advection might play a role in determining the phoretic velocity, since the time required for the solute to cross the length of the dimer in a shear flow (with shear rate $\dot{\gamma}$) via advection ($1/\dot{\gamma}$) was on the order of the time required

to cross via diffusion (a^2/D). The ratio of these two time scales defines a Peclet number for the imposed shear flow, $\dot{\gamma}a^2/D$. The shear flow Peclet number can be large enough to warrant consideration of the effect of advection on the solute concentration. For example, in blood vessels, $\dot{\gamma} \sim \mathrm{O}(10^2\ \mathrm{s}^{-1})$ are reasonable [26], and the shear rate in microchannels can be as high as $\dot{\gamma} \sim \mathrm{O}(10^4\ \mathrm{s}^{-1})$ [29]. Assuming D and L as before yields $\mathrm{Pe} \sim \mathrm{O}(10^{-1})$ to $\mathrm{O}(10^1)$, indicating advection by ambient flow can play a role in self-diffusiophoresis.

In this paper, we quantify the impact of an imposed flow on the dynamics of a self-diffusiophoretic colloidal particle. Specifically, we consider a model spherical Janus particle in a simple shear flow at small Pe to examine the first effects of advection on the dynamics of the particle. A similar mathematical problem of an inert sphere in shear flow and an external concentration or temperature gradient has also been analyzed at small Pe [2,30]. In that case, the key restriction in the analysis is that the shear flow and the imposed gradient must be orthogonal in order to maintain a steady linear gradient. However, for a self-diffusiophoretic particle, the concentration gradient is self-generated and therefore local. The solute concentration is uniform at large distances; hence, the orthogonality condition is no longer relevant, and there is no restriction on the direction of self-propulsion relative to the imposed flow.

Golestanian *et al.* [12] considered a model self-diffusiophoretic spherical particle in quiescent flow, where the axisymmetric surface reactivity and solute mobility differ over the particle surface, and the solute concentration evolves solely due to diffusion ($\mathrm{Pe} = 0$). To approximate the piecewise nature of the surface reactivity, α, and mobility, μ, of a Janus sphere, they define $\alpha = \sum_{l=0}^{\infty} \alpha_l P_l(\cos\theta')$ and $\mu = \sum_{l=0}^{\infty} \mu_l P_l(\cos\theta')$, where θ' is the polar angle from the direction of propulsion in a body-fixed frame, and α_l and μ_l are the coefficients for the surface reactivity and mobility, respectively, for each Legendre polynomial $P_l(\cos\theta')$. They found that the rectilinear velocity of the particle equals

$$\mathbf{U}_0 = \frac{\hat{\mathbf{d}}}{D} \sum_{l=0}^{\infty} \left(\frac{l+1}{2l+3} \right) \alpha_{l+1} \left[\frac{\mu_l}{2l+1} - \frac{\mu_{l+2}}{2l+5} \right], \quad (1)$$

where $\hat{\mathbf{d}}$ is the unit vector along the symmetry axis of the sphere.

In this paper, we will consider a simplified Janus particle, where the surface reactivity is $\alpha = \alpha_1 \cos\theta'$ and the mobility is constant, $\mu = \mu_0$. For the rest of the paper, α_1 and μ_0 shall be referred to as α and μ, respectively. Thus, (1) simplifies to $\mathbf{U}_0 = (\alpha\mu/3D)\hat{\mathbf{d}}$. For hard-sphere solute particles of size b, the repulsive excluded-volume interaction between the solute and the colloid gives $\mu = -k_B T b^2/2\eta$, where k_B is the Boltzmann constant, T is the temperature, and η is the viscosity [1]. Thus, the Janus colloid moves with its consuming face forward, down the self-generated gradient. Note, the phoretic velocity is solely along the symmetry axis of the particle. We will demonstrate that solute advection due to an imposed shear flow fundamentally alters the motion of the Janus particle, resulting in, for example, an O(Pe) cross-streamline drift.

In Sec. II, we present governing equations for a self-diffusiophoretic Janus particle in shear flow. In Sec. III, we solve for the concentration field surrounding the particle using matched asymptotic expansions and then compute the instantaneous particle velocity. In Sec. IV, we consider the resulting trajectory of a self-diffusiophoretic particle whose symmetry axis lies in the plane of shear. Conclusions are offered in Sec. V.

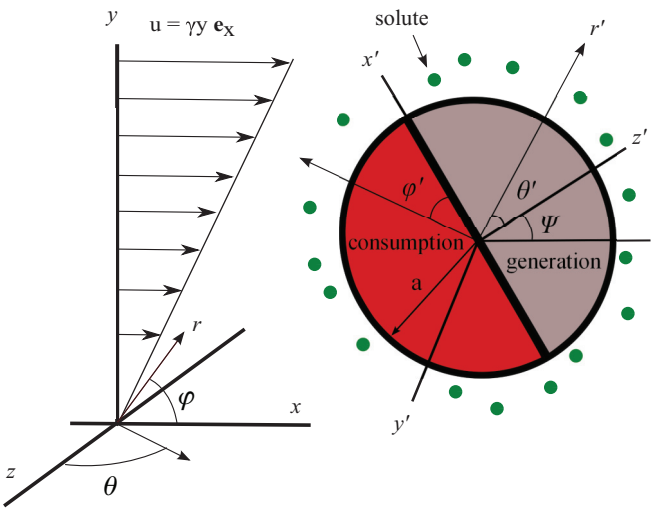

FIG. 1. (Color online) A spherical Janus particle of radius a immersed in an imposed shear flow, $\mathbf{u} = \dot{\gamma} y \mathbf{e}_x$. One side of the particle generates hard-sphere solute particles while the other side consumes them. The symmetry axis of the particle $\hat{\mathbf{d}}$ lies in the shear plane and is oriented at an angle ψ from the direction of the flow. The particle coordinate system is described as (r',θ',ϕ') (spherical polar) and (x',y',z') (Cartesian), while the laboratory fixed coordinate system is (r,θ,ϕ) and (x,y,z).

II. PROBLEM FORMULATION

We consider a spherical Janus particle of radius a in a Newtonian fluid at zero Reynolds number. At large distances from the particle, the fluid moves in simple shear flow, with velocity $\mathbf{u} = \dot{\gamma} y \mathbf{e}_x$, where $\mathbf{e}_x$ is a unit vector along the flow direction in a laboratory frame, and y is the coordinate in the velocity gradient direction $\mathbf{e}_y$ (Fig. 1). The particle generates and consumes hard-sphere solute particles over different portions of its surface. The solute concentration in the fluid far from the particle is uniform, c_∞. The particle moves with an instantaneous rectilinear velocity $\mathbf{U}$ and angular velocity $\boldsymbol{\Omega}$. We restrict the symmetry axis of the Janus particle to lie in the plane of shear and also neglect Brownian motion, although a preliminary discussion on the effects of the latter is presented in Sec. V.

We assume that solute molecules interact with the Janus particle via hard-sphere (excluded-volume) repulsion, on the length scale of the solute, which is much smaller than the size of the particle ($b \ll a$). Hence, the thin interfacial layer limit applies [1]. Here, the tangential solute gradient at the outer edge of the interfacial layer drives a diffusio-osmotic slip flow around the Janus particle. This slip velocity can be defined as [1]

$$\mathbf{v}_s = \mu\,(\mathbf{I} - \mathbf{nn}) \cdot \nabla c|_{r=a}, \quad (2)$$

where $\mathbf{n}$ is the unit vector normal to the particle surface, $\mathbf{I}$ is the identity tensor, and c is the solute concentration. Note, in (2) the location of $r = a$ corresponds strictly to the outer edge of the interfacial layer between the solute and the Janus particle. This can be taken as an effective boundary condition at the particle surface in the thin interfacial layer limit. For hard-sphere repulsion, $\mu < 0$, implying flow from high to low solute concentrations.

As mentioned previously, Golestanian *et al.* [12] utilized a sum of Legendre polynomials to describe the piecewise nature of the surface reactivity of a spherical Janus particle, $\alpha = \sum_{l=0}^{\infty} \alpha_l P_l(\cos\theta')$ [12]. We simplify this by using the first Legendre polynomial in the sequence, such that the surface reactivity equals $\alpha\cos(\theta')$. This provides a continuously varying reactivity with generation of solute for $0 < \theta' < \pi/2$ and consumption for $\pi/2 < \theta' < \pi$, which yields a concentration disturbance that varies as $1/r^2$ at $\mathrm{Pe} = 0$, characteristic of a diffusive dipole, where r is the distance from the center of the colloid. Note that this is also the long-range concentration decay of a true Janus particle with consuming and generating hemispheres. If the symmetry axis of the particle lies in the plane of shear, the reaction-diffusion boundary condition at the particle surface ($r = a$) in the laboratory fixed frame reads

$$-D\mathbf{n}\cdot\nabla c = \alpha\sin(\theta)\cos(\phi - \psi), \tag{3}$$

where ψ is the angle of the symmetry axis, or director, to the flow direction (Fig. 1). Equation (3) specifies that the diffusive concentration flux at the surface of the particle is equal to the flux due to reaction, as defined by the surface reactivity. The application of (2) and (3) as effective boundary conditions at the outer edge of the interfacial layer is valid provided Pe is not large [22]. At $\mathrm{Pe} = 0$ (no advection), the particle translates at a velocity $\mathbf{U}_0 = (\alpha\mu/3D)\hat{\mathbf{d}}$, where the director $\hat{\mathbf{d}} = \cos\psi\,\mathbf{e}_x + \sin\psi\,\mathbf{e}_y$.

The solute concentration around the particle obeys the advection-diffusion equation

$$\frac{\partial c}{\partial t} + \mathbf{u}\cdot\nabla c = D\nabla^2 c. \tag{4}$$

At large distances, c tends to the uniform background concentration c_∞. The value of c_∞ plays no dynamical role in what follows, hence we define a concentration disturbance $C = c - c_\infty$. The disturbance is normalized to $\alpha a/D$, the characteristic concentration scale due to the balance between surface reaction and bulk diffusion. The flow velocity $\mathbf{u}$ is nondimensionalized by the speed of imposed shear, $\dot\gamma a$. Distance is nondimensionalized by the colloid radius, a. The characteristic time for the evolution of the solute concentration due to the phoretic motion of the Janus particle is the time taken for the Janus particle to travel a full body length, since at that point it will be clear of its self-imposed concentration gradient. Hence time t is nondimensionalized by a/U_0, where $U_0 = \alpha\mu/D$. This yields the nondimensionalized advection-diffusion equation,

$$\mathrm{Pe}_{\mathrm{tr}}\frac{\partial \bar C}{\partial \bar t} + \mathrm{Pe}_{\mathrm{sh}}\bar{\mathbf{u}}\cdot\bar\nabla\bar C = \bar\nabla^2\bar C, \tag{5}$$

where for any dimensional variable χ, $\bar\chi$ is its dimensionless counterpart. In (5), $\mathrm{Pe}_{\mathrm{tr}}$ is the Peclet number associated with the translation of the sphere, $\mathrm{Pe}_{\mathrm{tr}} = U_0 a/D$, and $\mathrm{Pe}_{\mathrm{sh}}$ is the Peclet number associated with the shear flow, $\mathrm{Pe}_{\mathrm{sh}} = \dot\gamma a^2/D$. Given that $\mathrm{Pe}_{\mathrm{tr}}$ is typically small, transient changes in the concentration gradient due to the translation of the Janus particle can be neglected, and the velocity field is due solely to the imposed shear flow, yielding the steady-state advection-diffusion equation:

$$\mathrm{Pe}_{\mathrm{sh}}\bar{\mathbf{u}}\cdot\bar\nabla\bar C = \bar\nabla^2\bar C, \tag{6}$$

where the fluid velocity vector

$$\bar{\mathbf{u}} = \bar u_r\mathbf{e}_r + \bar u_\theta\mathbf{e}_\theta + \bar u_\phi\mathbf{e}_\phi, \tag{7}$$

where $\mathbf{e}_r$, $\mathbf{e}_\theta$, and $\mathbf{e}_\phi$ are the radial, polar, and azimuthal unit vectors, respectively, in the laboratory frame, and the velocity components are [2]

$$\begin{aligned}
\bar u_r &= \left(-\frac{1}{2\bar r^2} + \frac{\bar r}{2}\right)\sin 2\phi\,\sin^2\theta,\\
\bar u_\theta &= \left(-\frac{1}{2\bar r^4} + \frac{\bar r}{2}\right)\sin 2\phi\,\cos\theta\,\sin\theta,\\
\bar u_\phi &= -\frac{\bar r}{2}\sin\theta + \left(-\frac{1}{2\bar r^4} + \frac{\bar r}{2}\right)\cos 2\phi\,\sin\theta.
\end{aligned} \tag{8}$$

Henceforth, $\mathrm{Pe}_{\mathrm{sh}}$ shall be referred to as Pe.

From the solution of (6), our aim is to determine the rectilinear velocity of the particle, $\mathbf{U}$, as well as the angular velocity of the particle, $\mathbf{\Omega}$, induced by the self-generated solute concentration gradient. We define the dimensionless velocities $\bar{\mathbf{U}} = \mathbf{U}/U_0$ and $\bar{\mathbf{\Omega}} = \mathbf{\Omega}a/U_0$. These quantities can be found as quadratures of the surface slip velocity [31],

$$\bar{\mathbf{U}} = -\frac{1}{4\pi}\int_S \bar{\mathbf{v}}_s\,dS \quad\text{and}\quad \bar{\mathbf{\Omega}} = -\frac{3}{8\pi}\int_S \bar{\mathbf{v}}_s\times\mathbf{n}\,dS, \tag{9}$$

where $\bar{\mathbf{v}}_s = (\mathbf{I} - \mathbf{nn})\cdot\bar\nabla\bar C|_{\bar r=1}$.

In this paper, we focus on excluded-volume interactions to provide a concrete physical interpretation for the effect of ambient shear on self-diffusiophoresis. However, it should be noted that the thin-interfacial-layer formalism utilized here is valid for an arbitrary short-range interaction potential (Φ) between the solute and Janus particle, with the (dimensional) mobility given by $\mu = (k_BT/\eta)\int_0^\infty l[1 - e^{-\Phi(l)/k_BT}]dl$, where the integral is across the interfacial layer, and l is a local coordinate normal to the particle surface [1,22].

III. MATCHED ASYMPTOTIC EXPANSIONS

The steady advection-diffusion equation in linear flows is singular at small Pe [2,32]. The solution domain can be divided into two regions: an inner region, $\bar r \sim O(1)$, where diffusion dominates advection, and an outer region, $\bar r \gg 1$, where diffusion and advection are balanced. More precisely, the balance occurs at $\bar r \sim O(\mathrm{Pe}^{-1/2})$, hence we define an outer radial coordinate $\bar\rho = \bar r\,\mathrm{Pe}^{1/2}$, where $\bar\rho \sim O(1)$ as $\mathrm{Pe}\to 0$. We define the inner region solute concentration as $\bar C$ and the outer region solute concentration as $\bar C^*$. The solute concentrations in the two regions are then matched in a domain of overlap. We pose expansions of the solute concentration in the inner

and outer regions as

$$\bar{C} = f_0(\mathrm{Pe})\bar{C}_0 + f_1(\mathrm{Pe})\bar{C}_1 + f_2(\mathrm{Pe})\bar{C}_2 + \cdots, \quad (10)$$

$$\bar{C}^* = F_0(\mathrm{Pe})\bar{C}_0^* + F_1(\mathrm{Pe})\bar{C}_1^* + F_2(\mathrm{Pe})\bar{C}_2^* + \cdots, \quad (11)$$

respectively, where $f_{n+1}/f_n \to 0$ as $\mathrm{Pe} \to 0$ and $F_{n+1}/F_n \to 0$ as $\mathrm{Pe} \to 0$.

For the first term of the inner expansion, $f_0(\mathrm{Pe}) = 1$, since the leading contribution to $\bar{C}$ is $\mathrm{O}(\mathrm{Pe}^0)$ from the reaction-diffusion boundary condition (3). Thus, inserting (10) into (6) yields $\bar{\nabla}^2\bar{C}_0 = 0$, demonstrating that the solute concentration evolves solely via diffusion at $\mathrm{Pe} = 0$. The solution is

$$\bar{C}_0 = \sum_{l=0}^{\infty}\sum_{m=0}^{l}(A_l\bar{r}^l + B_l\bar{r}^{-(l+1)})(C_m\cos m\phi + D_m\sin m\phi) \times P_l^m(\cos\theta), \quad (12)$$

where $P_l^m(\cos\theta)$ is an associated Legendre polynomial of degree l and order m. The solution must decay as $\bar{r} \to \infty$ and obeys the reaction-diffusion condition (3) at $\bar{r} = 1$. This yields

$$\bar{C}_0 = \frac{1}{2\bar{r}^2}(\cos\psi\cos\phi + \sin\psi\sin\phi)\sin\theta. \quad (13)$$

The $1/\bar{r}^2$ decay shows that the disturbance of the inner solute concentration is that of a diffusive dipole at $\mathrm{Pe} = 0$. Note that the same long-range concentration decay would be found for a particle with distinct consuming and generating hemispheres. Hence, our simplified model captures, albeit crudely, the essential features of a true Janus particle.

Writing $\bar{C}_0$ in terms of the outer coordinate, $\bar{\rho}$, we find $\bar{C}_0 \sim \mathrm{Pe}/\bar{\rho}^2$. Thus, the first term of the outer expansion is $\mathrm{O}(\mathrm{Pe})$, $F_0(\mathrm{Pe}) = \mathrm{Pe}$. Hence, we assert that the second-order term of the inner expansion is $\mathrm{O}(\mathrm{Pe})$, $f_1(\mathrm{Pe}) = \mathrm{Pe}$. From (6) and (10), the $\mathrm{O}(\mathrm{Pe})$ inner concentration, $\bar{C}_1$, satisfies

$$\nabla^2\bar{C}_1 = \bar{\mathbf{u}}\cdot\bar{\nabla}\bar{C}_0. \quad (14)$$

The right-hand side represents the advection of the O(1) inner concentration, $\bar{C}_0$, by the shear flow. Substituting (13) and (7) into (14) yields

$$\begin{aligned}\nabla^2\bar{C}_1 = \Bigg\{&\sin\phi\cos\psi\left[\sin\theta\left(-\frac{1}{8\bar{r}^2}-\frac{5}{8\bar{r}^5}+\frac{1}{2\bar{r}^7}\right)+\sin\theta\cos^2\theta\left(-\frac{3}{8\bar{r}^2}+\frac{5}{8\bar{r}^5}-\frac{1}{4\bar{r}^7}\right)\right]\\ &+\sin 3\phi\cos\psi\left[\sin\theta\left(\frac{3}{8\bar{r}^2}-\frac{5}{8\bar{r}^5}+\frac{1}{4\bar{r}^7}\right)+\sin\theta\cos^2\theta\left(-\frac{3}{8\bar{r}^2}+\frac{5}{8\bar{r}^5}-\frac{1}{4\bar{r}^7}\right)\right]\\ &+\cos\phi\sin\psi\left[\sin\theta\left(-\frac{1}{8\bar{r}^2}-\frac{5}{8\bar{r}^5}+\frac{1}{2\bar{r}^7}\right)+\sin\theta\cos^2\theta\left(-\frac{3}{8\bar{r}^2}+\frac{5}{8\bar{r}^5}-\frac{1}{4\bar{r}^7}\right)\right]\\ &+\cos 3\phi\sin\psi\left[\sin\theta\left(-\frac{3}{8\bar{r}^2}+\frac{5}{8\bar{r}^5}-\frac{1}{4\bar{r}^7}\right)+\sin\theta\cos^2\theta\left(\frac{3}{8\bar{r}^2}-\frac{5}{8\bar{r}^5}+\frac{1}{4\bar{r}^7}\right)\right]\Bigg\}. \end{aligned} \quad (15)$$

The particular solution to (15) is

$$\begin{aligned}\bar{C}_{1,p} = \Bigg(&\cos\psi\Bigg\{\sin\phi\left[P_1^1(\cos\theta)\left(-\frac{1}{10}+\frac{1}{8\bar{r}^3}-\frac{1}{40\bar{r}^5}\right)+P_3^1(\cos\theta)\left(-\frac{1}{240}+\frac{1}{72\bar{r}^3}+\frac{1}{240\bar{r}^5}\right)\right]\\ &+\sin 3\phi\ P_3^3(\cos\theta)\left(\frac{1}{480}+\frac{1}{144\bar{r}^3}+\frac{1}{480\bar{r}^5}\right)\Bigg\}\\ &+\sin\psi\Bigg\{\cos\phi\left[P_1^1(\cos\theta)\left(-\frac{1}{10}+\frac{1}{8\bar{r}^3}-\frac{1}{40\bar{r}^5}\right)+P_3^1(\cos\theta)\left(-\frac{1}{240}+\frac{1}{72\bar{r}^3}+\frac{1}{240\bar{r}^5}\right)\right]\\ &+\sin 3\phi\ P_3^3(\cos\theta)\left(-\frac{1}{480}+\frac{1}{144\bar{r}^3}+\frac{1}{480\bar{r}^5}\right)\Bigg\}\Bigg). \end{aligned} \quad (16)$$

The complementary solution to (15) is

$$\bar{C}_{1,c} = \sum_{l=0}^{\infty}\sum_{m=0}^{l}(A_l\bar{r}^l + B_l\bar{r}^{-(l+1)})(C_m\cos m\phi + D_m\sin m\phi)\,P_l^m(\cos\theta). \quad (17)$$

To determine the constants A_l, B_l, C_m, and D_m, the inner and matching boundary conditions must be applied. The latter requires that $A_l = 0$ for $l > 0$ so that terms greater than $\mathrm{O}(\mathrm{Pe})$ are not generated in the outer region. By considering the inner boundary condition at $\mathrm{O}(\mathrm{Pe})$, which from (3) reads $\mathbf{n}\cdot\nabla\bar{C}_1 = \mathbf{0}$, the overall $\mathrm{O}(\mathrm{Pe})$ inner solution can be determined as

$$\begin{aligned}\bar{C}_1 = \Bigg(&\cos\psi\Bigg\{\sin\phi\left[P_1^1(\cos\theta)\left(-\frac{1}{10}-\frac{1}{8\bar{r}^2}+\frac{1}{8\bar{r}^3}-\frac{1}{40\bar{r}^5}\right)+P_3^1(\cos\theta)\left(-\frac{1}{240}+\frac{1}{72\bar{r}^3}-\frac{1}{64\bar{r}^4}+\frac{1}{240\bar{r}^5}\right)\right]\\ &+\sin 3\phi\ P_3^3(\cos\theta)\left(\frac{1}{480}+\frac{1}{144\bar{r}^3}+\frac{1}{128\bar{r}^4}+\frac{1}{480\bar{r}^5}\right)\Bigg\}\end{aligned}$$

$$+\sin\psi\left\{\cos\phi\left[P_1^1(\cos\theta)\left(-\frac{1}{10}-\frac{1}{8\bar{r}^2}+\frac{1}{8\bar{r}^3}-\frac{1}{40\bar{r}^5}\right)+P_3^1(\cos\theta)\left(-\frac{1}{240}+\frac{1}{72\bar{r}^3}-\frac{1}{64\bar{r}^4}+\frac{1}{240\bar{r}^5}\right)\right]\right.$$
$$\left.+\sin 3\phi\ P_3^3(\cos\theta)\left(-\frac{1}{480}+\frac{1}{144\bar{r}^3}-\frac{1}{128\bar{r}^4}+\frac{1}{480\bar{r}^5}\right)\right\}\Bigg). \tag{18}$$

The inner limit ($\bar{\rho}\to 0$) of the first outer concentration term, $\bar{C}_0^*$, matches the outer limit ($\bar{r}\to\infty$) of $\bar{C}_0+\mathrm{Pe}\bar{C}_1$, where

$$\bar{C}_0+\mathrm{Pe}\bar{C}_1=\mathrm{Pe}\Bigg(\cos\psi\left\{-\sin\phi\left[\left(\frac{1}{2\bar{\rho}^2}+\frac{1}{10}\right)P_1^1(\cos\theta)+\frac{1}{240}P_3^1(\cos\theta)\right]+\frac{1}{480}\sin 3\phi\ P_3^3(\cos\theta)\right\}$$
$$+\sin\psi\left\{-\sin\phi\left[\left(\frac{1}{2\bar{\rho}^2}+\frac{1}{10}\right)P_1^1(\cos\theta)+\frac{1}{240}P_3^1(\cos\theta)\right]-\frac{1}{480}\sin 3\phi\ P_3^3(\cos\theta)\right\}\Bigg) \tag{19}$$

to O(Pe) in terms of the outer coordinate $\bar{\rho}$. Inserting (11) into (6), and using (7) and (8), the governing equation for $\bar{C}_0^*$ is

$$\bar{\nabla}_{\bar{\rho}}^2\bar{C}_0^*=\hat{y}\frac{\partial\bar{C}_0^*}{\partial\hat{x}}, \tag{20}$$

where $\hat{x}=\mathrm{Pe}^{1/2}\bar{x}$ and $\hat{y}=\mathrm{Pe}^{1/2}\bar{y}$, respectively, and $\bar{\nabla}_{\bar{\rho}}$ is the gradient operator in terms of the outer radial coordinate $\bar{\rho}$. The above equation represents the balance of solute diffusion and advection by ambient shear. The disturbance to the ambient shear flow due to the presence of the particle appears at higher orders in the outer region. To leading order, the Janus particle acts as a concentration dipole at the scale of the outer region. The solution for a sustained concentration monopole in shear flow was found by Elrick as [33]

$$C_E=\frac{1}{2\sqrt{\pi}}\int_0^\infty\frac{dS}{S^{3/2}\left(1+\frac{1}{12}S^2\right)^{1/2}}\times\exp\left[-\left(\frac{\left(\hat{x}-\frac{1}{2}\hat{y}S\right)^2}{4S\left(1+\frac{1}{12}S^2\right)}+\frac{\hat{y}^2+\hat{z}^2}{4S}\right)\right], \tag{21}$$

where $\hat{z}=\mathrm{Pe}^{1/2}\bar{z}$. Following Leal [2], the dipole solution can be constructed as $\bar{C}_0^*=2A\hat{\mathbf{d}}\cdot\nabla C_E$, where $2A$ is the dipole strength, which will be found via matching. Hence, using $\hat{\mathbf{d}}=\cos\psi\mathbf{e}_x+\sin\psi\mathbf{e}_y$, we find

$$\bar{C}_0^*=2A\int_0^\infty\left[\cos\psi\frac{\partial}{\partial\hat{x}}+\sin\psi\frac{\partial}{\partial\hat{y}}\right]\left\{\frac{1}{\left(1+\frac{1}{12}S^2\right)^{\frac{1}{2}}S^{\frac{3}{2}}}\exp\left[-\left(\frac{\left(\hat{x}-\frac{1}{2}\hat{y}S\right)^2}{4S\left(1+\frac{1}{12}S^2\right)}+\frac{\hat{y}^2+\hat{z}^2}{4S}\right)\right]dS\right\}. \tag{22}$$

To match (6) to (19), we need the limit of (22) as $\bar{\rho}\to 0$. It can be shown that (see the Appendix)

$$\bar{C}_0^*=A\left\{\frac{4\pi}{\bar{\rho}^2}P_1^1(\cos\theta)(\sin\psi\sin\phi+\cos\psi\cos\phi)-\frac{4\sqrt{\pi}}{5}P_1^1(\cos\theta)(\sin\psi\cos\phi+\cos\psi\sin\phi)\right.$$
$$+\frac{\sqrt{\pi}}{30}P_3^1(\cos\theta)(\sin\psi\cos\phi+\cos\psi\sin\phi)+\frac{\sqrt{\pi}}{60}P_3^3(\cos\theta)(\sin\psi\cos 3\phi+\cos\psi\sin 3\phi)$$
$$\left.+\bar{\rho}P_1^1(\cos\theta)(-0.671\sin\psi\sin\phi+0.683\sin\psi\cos\phi+0.683\cos\psi\sin\phi+0.479\cos\psi\cos\phi)\right\}+O(\bar{\rho}^2) \tag{23}$$

as $\bar{\rho}\to 0$, where the numerical coefficients are quoted to three decimal places.

Matching (23) to (19) yields $A=1/(8\sqrt{\pi})$. The terms of $O(\bar{\rho})$ in (23) match to the next (third) term in the inner region, which is therefore O($\mathrm{Pe}^{3/2}$) since $\mathrm{Pe}\bar{\rho}=\mathrm{Pe}^{3/2}\bar{r}$. Thus $f_2=\mathrm{Pe}^{3/2}$. The third term in the inner region, $\bar{C}_2$, satisfies $\bar{\nabla}^2\bar{C}_2=0$. At this order, the inner solute concentration evolves solely due to diffusion as there is no term of the inner region solute concentration of O($\mathrm{Pe}^{1/2}$) to balance diffusion with advection. The solution for $\bar{C}_2$ is simply

$$\bar{C}_2=\frac{1}{8\sqrt{\pi}}\left(\bar{r}+\frac{1}{2\bar{r}^2}\right)(0.683\sin\psi\cos\phi+0.479\cos\psi\cos\phi-0.671\sin\psi\sin\phi+0.683\cos\psi\sin\phi), \tag{24}$$

where the numerical coefficients in (24) are again quoted to three decimal places. Thus, the inner concentration through O($\mathrm{Pe}^{3/2}$) equals

$$\bar{C}=\frac{1}{2r^2}(\cos\psi\cos\phi+\sin\psi\sin\phi)P_1^1(\cos\theta)$$
$$+\mathrm{Pe}\Bigg(\cos\psi\left\{\sin\phi\left[P_1^1(\cos\theta)\left(-\frac{1}{10}-\frac{1}{8\bar{r}^2}+\frac{1}{8\bar{r}^3}-\frac{1}{40\bar{r}^5}\right)+P_3^1(\cos\theta)\left(-\frac{1}{240}+\frac{1}{72\bar{r}^3}-\frac{1}{64\bar{r}^4}+\frac{1}{240\bar{r}^5}\right)\right]\right.$$
$$\left.+\sin 3\phi\ P_3^3(\cos\theta)\left(\frac{1}{480}+\frac{1}{144\bar{r}^3}+\frac{1}{128\bar{r}^4}+\frac{1}{480\bar{r}^5}\right)\right\}$$

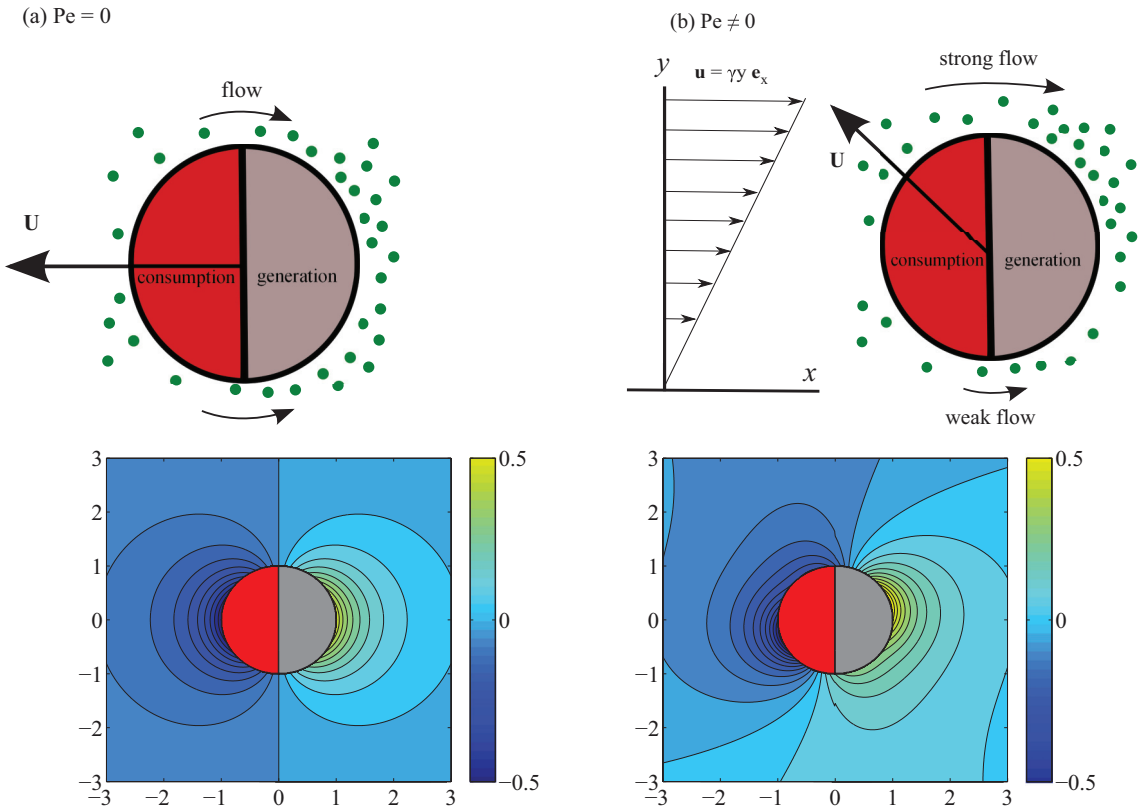

FIG. 2. (Color online) Solute concentration around a self-diffusiophoretic particle aligned along the flow direction of the imposed shear, $\psi = 0$. (a) The solute concentration at $\mathrm{Pe} = 0$ is dependent solely on solute diffusion and is axially symmetric. This is sketched in the top image of (a), and the bottom image of (a) plots the solute concentration in the shear plane for $\mathrm{Pe} = 0$ from (13). The color scheme indicates increasing concentration in green (light gray) and decreasing concentration in blue (dark gray). As a result of the axial symmetry, the particle moves solely along its symmetry axis. (b) In a shear flow ($\mathrm{Pe} \neq 0$), the axial symmetry is broken as the shear flow aids and restricts solute flux on the bottom and top halves of the particle, respectively. The resulting top-bottom asymmetry results in particle migration across fluid streamlines, as depicted in the top image of (b). The bottom image of (b) plots the solute concentration at $\mathrm{Pe} = 0.5$ from (25): the broken symmetry is clearly evident.

$$+ \sin\psi \left\{ \cos\phi \left[P_1^1(\cos\theta)\left(-\frac{1}{10} - \frac{1}{8\bar{r}^2} + \frac{1}{8\bar{r}^3} - \frac{1}{40\bar{r}^5}\right) + P_3^1(\cos\theta)\left(-\frac{1}{240} + \frac{1}{72\bar{r}^3} - \frac{1}{64\bar{r}^4} + \frac{1}{240\bar{r}^5}\right)\right] \right.$$
$$\left. + \cos 3\phi \; P_3^3(\cos\theta)\left(-\frac{1}{480} - \frac{1}{144\bar{r}^3} - \frac{1}{128\bar{r}^4} - \frac{1}{480\bar{r}^5}\right)\right\}\Bigg)$$
$$+ \frac{\mathrm{Pe}^{3/2}}{8\sqrt{\pi}} P_1^1(\cos\theta)\left(\bar{r} + \frac{1}{2\bar{r}^2}\right)\left(\cos\phi\,(0.683\sin\psi + 0.479\cos\psi) + \sin\phi\,(-0.671\sin\psi + 0.683\cos\psi)\right) + \mathrm{O}(\mathrm{Pe}^2). \quad (25)$$

The inner concentration (25) will now be used to compute the phoretic particle velocity through $\mathrm{O}(\mathrm{Pe}^{3/2})$.

IV. PARTICLE MOTION AND TRAJECTORY ANALYSIS

Substituting (25) into (9) and performing the required angular integration, we find that the particle velocity $\bar{\mathbf{U}} = \bar{U}_x\mathbf{e}_x + \bar{U}_y\mathbf{e}_y + \bar{U}_z\mathbf{e}_z$, where

$$\bar{U}_x = \frac{1}{3}\cos\psi - \frac{\mathrm{Pe}}{12}\sin\psi + \mathrm{Pe}^{\frac{3}{2}}(0.034\cos\psi + 0.048\sin\psi),$$
$$\bar{U}_y = \frac{1}{3}\sin\psi - \frac{\mathrm{Pe}}{12}\cos\psi + \mathrm{Pe}^{\frac{3}{2}}(0.048\cos\psi - 0.046\sin\psi),$$
$$\bar{U}_z = 0. \quad (26)$$

Equation (26) shows that solute advection due to ambient shear ($\mathrm{Pe} \neq 0$) fundamentally alters the motion of the self-propelled particle from its motion in quiescent flow ($\mathrm{Pe} = 0$). Note that $\bar{U}_z = 0$; since the particle symmetry axis lies in the plane of shear, there is no component of particle velocity along the vorticity axis of the ambient shear. Consider, for example, the case $\psi = 0$ in which the symmetry axis is aligned with the flow. From (26),

$$\bar{U}_x(\psi = 0) = \frac{1}{3} + 0.034\,\mathrm{Pe}^{\frac{3}{2}},$$
$$\bar{U}_y(\psi = 0) = -\frac{\mathrm{Pe}}{12} + 0.048\,\mathrm{Pe}^{\frac{3}{2}}. \quad (27)$$

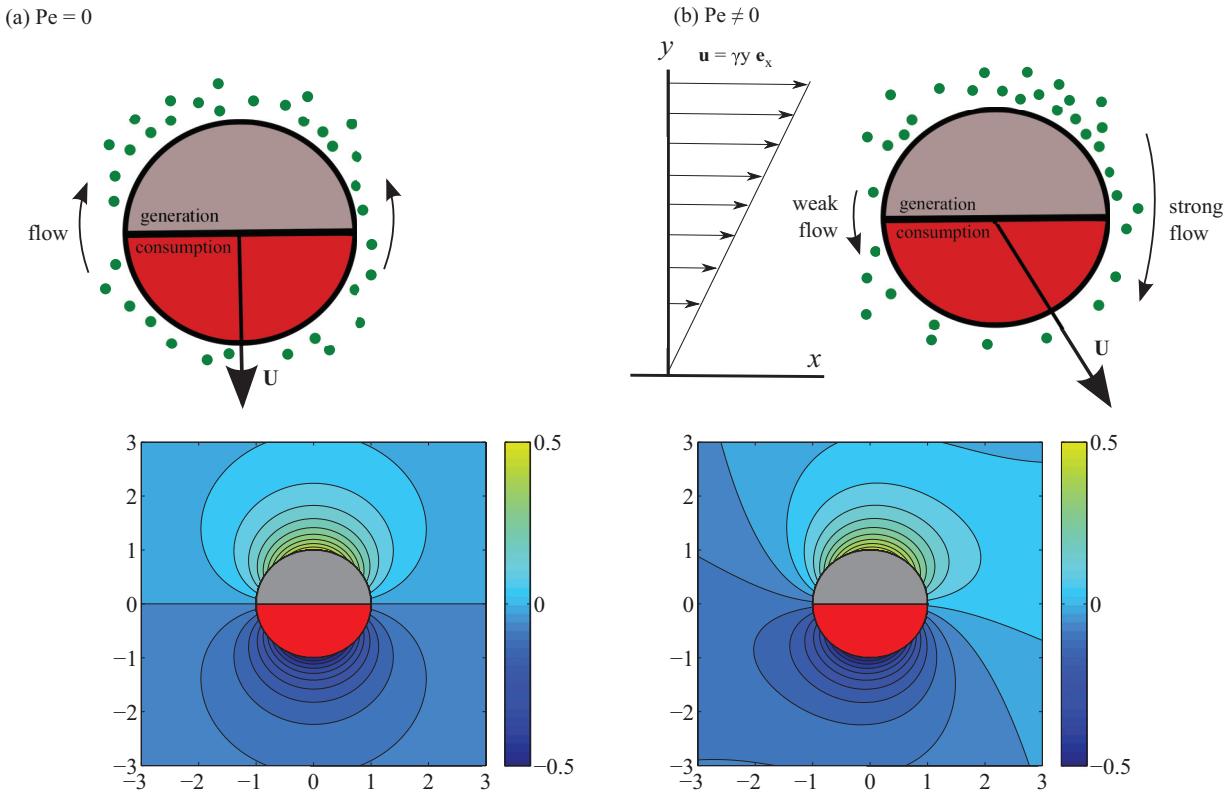

FIG. 3. (Color online) Solute concentration around a self-diffusiophoretic particle aligned along the gradient direction of the imposed shear, $\psi = \pi/2$. (a) The solute concentration at $\mathrm{Pe} = 0$ is dependent solely on diffusion and is therefore axially symmetric, leading to particle motion solely in the velocity gradient y direction. This is sketched in the top image of (a), and the bottom image of (a) plots the solute concentration in the shear plane for $\mathrm{Pe} = 0$ (color scheme is the same as Fig. 2). (b) In a shear flow ($\mathrm{Pe} \neq 0$), the left-right symmetry of the concentration field is broken, inducing an O(Pe) phoretic velocity contribution along the flow x direction, as depicted in the top figure of (b). The asymmetric concentration is plotted in the bottom figure of (b) for $\mathrm{Pe} = 0.5$ from (25).

The velocity of the particle is entirely along its symmetry axis in the absence of advection ($\mathrm{Pe} = 0$): $\bar{U}_x = 1/3$ and $\bar{U}_y = 0$. Recall that the particle velocity has been normalized by $\alpha\mu/D$, which is negative for hard-sphere solute-particle interactions. Hence, $\bar{U}_x = 1/3$ corresponds to particle translation in the negative $\mathbf{e}_x$ direction: the particle propels down the concentration gradient with the consuming face forward. With advection ($\mathrm{Pe} \neq 0$) there is an O(Pe) velocity contribution perpendicular to the symmetry axis, resulting in cross-streamline migration in the y direction. Physically, the shear flow breaks the axial symmetry of the solute concentration around the colloid. With the Janus particle oriented at $\psi = 0$ (Fig. 2), the diffusive flux of the solute on the top hemisphere is resisted by the shear flow, effectively increasing the concentration gradient and slip flow from consuming to generating sections. On the bottom hemisphere, the diffusive flux of the solute is aided by the shear flow, resulting in a weaker concentration gradient and hence slip flow. The resulting top-bottom asymmetry (y direction) in the concentration gradient induces a net O(Pe) downward diffusio-osmotic thrust; as the colloid is force-free it drifts to increasing y. At $\mathrm{O}(\mathrm{Pe}^{3/2})$, there is an enhancement in the velocity in the flow direction and reduction in cross-streamline drift.

One might suspect that the predicted cross-streamline migration invalidates the assumption of a steady-state solute concentration distribution (6). Indeed, as the particle traverses streamlines of the imposed shear, it encounters a spatially varying flow, which would entail a transient readjustment of solute concentration. However, the time scale to establish a steady concentration profile is set by the diffusion time a^2/D, whereas the time scale for cross-streamline migration is $a/(U_0\mathrm{Pe}_{\mathrm{sh}})$ (where $\mathrm{Pe}_{\mathrm{sh}} = \dot{\gamma}a^2/D$ is the shear flow Peclet number): their ratio $(a^2/D)/[a/(U_0\mathrm{Pe}_{\mathrm{sh}})] = \mathrm{Pe}_{\mathrm{tr}}\mathrm{Pe}_{\mathrm{sh}}$, where $\mathrm{Pe}_{\mathrm{tr}} = U_0 a/D$ is the Peclet number due to particle translation. Hence, the assumption of a steady solute concentration during cross-streamline migration requires $\mathrm{Pe}_{\mathrm{tr}}\mathrm{Pe}_{sh} \ll 1$, which, since $\mathrm{Pe}_{\mathrm{tr}} \ll 1$ under typical conditions, is a less stringent requirement than the assumed limit $\mathrm{Pe}_{\mathrm{sh}} \ll 1$. Thus, it is valid to assume a steady solute concentration profile.

Another important case is $\psi = \pi/2$, where the particle symmetry axis is perpendicular to the flow. Here, the velocity of the particle is

$$\begin{aligned} \bar{U}_x(\psi = \pi/2) &= -\frac{\mathrm{Pe}}{12} + 0.048\,\mathrm{Pe}^{\frac{3}{2}}, \\ \bar{U}_y(\psi = \pi/2) &= \frac{1}{3} - 0.046\,\mathrm{Pe}^{\frac{3}{2}}. \end{aligned} \tag{28}$$

At $\mathrm{Pe} = 0$, the particle moves solely in the flow gradient direction, $\bar{U}_y = 1/3$. However, the left-right symmetry of the concentration gradient is broken at $\mathrm{Pe} \neq 0$, resulting in an

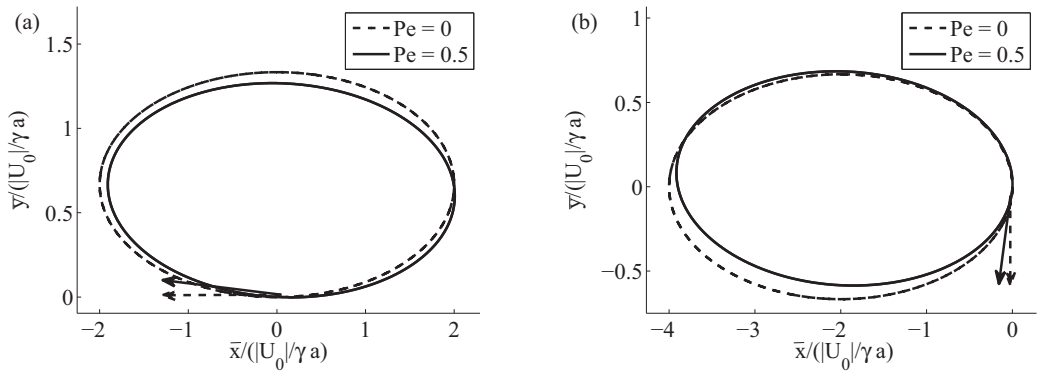

FIG. 4. Planar trajectory of a self-diffusiophoretic particle in a shear flow: (a) the particle is initially aligned with the shear flow ($\psi_0 = 0$); and (b) the particle is aligned with the flow gradient ($\psi_0 = \pi/2$). Trajectories are plotted for Pe = 0 and 0.5; in both cases, the trajectories are elliptical; however, the area of the orbit decreases at finite Pe. The arrows depict the initial translation direction of the particle.

O(Pe) motion in the flow direction ($\mathbf{e}_x$), as seen in Fig. 3. At O($\mathrm{Pe}^{3/2}$), there is a reduction in the velocity in the flow direction as well as a reduction in the velocity in the flow gradient direction.

Substituting (25) into (9), we also find that $\bar{\mathbf{\Omega}} = \mathbf{0}$, which means that the sphere experiences no rotation due to the diffusio-osmotic slip flow. Thus, the torque-free colloid will simply rotate with the ambient shear, at angular velocity $(\dot{\gamma}/2)\mathbf{e}_z$. Thus, the director remains in the shear plane, and its angle to the flow direction evolves as $\psi(t) = \psi_0 - \frac{\dot{\gamma}t}{2}$, where ψ_0 is the initial orientation. The total velocity of the particle, $\mathbf{U}_{\mathrm{tot}}$ say, is thus the sum of phoretic particle velocity (26) and the ambient flow at the particle center, $\dot{\gamma}\, y\mathbf{e}_x$. Normalizing $\mathbf{U}_{\mathrm{tot}}$ by the characteristic shear speed $\dot{\gamma}a$ yields the dimensionless total time-dependent particle velocity, $\bar{\mathbf{U}}_{\mathrm{tot}}(\tilde{t}) = \bar{U}_{\mathrm{tot},x}(\tilde{t})\mathbf{e}_x + \bar{U}_{\mathrm{tot},y}(\tilde{t})\mathbf{e}_y$, where

$$\bar{U}_{x,\mathrm{tot}}(\tilde{t}) = \bar{y} + \frac{U_0}{\dot{\gamma}a}\left\{\frac{1}{3}\cos\left(\phi_0 - \frac{\tilde{t}}{2}\right) - \frac{\mathrm{Pe}}{12}\sin\left(\phi_0 - \frac{\tilde{t}}{2}\right) + \mathrm{Pe}^{3/2}\left[0.034\cos\left(\phi_0 - \frac{\tilde{t}}{2}\right) + 0.048\sin\left(\phi_0 - \frac{\tilde{t}}{2}\right)\right]\right\},$$

$$\bar{U}_{y,\mathrm{tot}}(\tilde{t}) = \frac{U_0}{\dot{\gamma}a}\left\{\frac{1}{3}\sin\left(\phi_0 - \frac{\tilde{t}}{2}\right) - \frac{\mathrm{Pe}}{12}\cos\left(\phi_0 - \frac{\tilde{t}}{2}\right) + \mathrm{Pe}^{3/2}\left[0.048\cos\left(\phi_0 - \frac{\tilde{t}}{2}\right) - 0.046\sin\left(\phi_0 - \frac{\tilde{t}}{2}\right)\right]\right\}, \quad (29)$$

where $\tilde{t} = \dot{\gamma}t$. From integration of (29), the particle trajectory in the x-y plane is given by $\bar{\mathbf{r}}(\tilde{t}) = \bar{x}(\tilde{t})\mathbf{e}_x + \bar{y}(\tilde{t})\mathbf{e}_y$, where

$$\bar{x}(\tilde{t}) = \frac{U_0}{\gamma a}\left\{-2\sin\left(\psi_0 - \frac{\tilde{t}}{2}\right) + \frac{\mathrm{Pe}}{6}\cos\left(\psi_0 - \frac{\tilde{t}}{2}\right) - \mathrm{Pe}^{3/2}\left[-0.122\sin\left(\psi_0 - \frac{\tilde{t}}{2}\right) + 0.096\cos\left(\psi_0 - \frac{\tilde{t}}{2}\right)\right]\right\}, \quad (30)$$

$$\bar{y}(\tilde{t}) = \frac{U_0}{\gamma a}\left\{\frac{2}{3}\cos\left(\psi_0 - \frac{\tilde{t}}{2}\right) + \frac{\mathrm{Pe}}{6}\sin\left(\psi_0 - \frac{\tilde{t}}{2}\right) - \mathrm{Pe}^{3/2}\left[0.096\sin\left(\psi_0 - \frac{\tilde{t}}{2}\right) + 0.095\cos\left(\psi_0 - \frac{\tilde{t}}{2}\right)\right]\right\}, \quad (31)$$

where we have assumed the particle starts at the center of flow, $(\bar{x},\bar{y}) = (0,0)$ at $\tilde{t} = 0$. The particle trajectory is elliptical (Fig. 4), with a major axis along $\mathbf{e}_x$ of $a = U_0/\dot{\gamma}a(2 - 0.012\,\mathrm{Pe}^{1/2} + 0.003\,\mathrm{Pe} - 0.008\,\mathrm{Pe}^{3/2}) + \mathrm{O}(\mathrm{Pe}^2)$ and a minor axis along $\mathbf{e}_y$ of $b = U_0/\dot{\gamma}a(2/3 - 0.095\,\mathrm{Pe}^{3/2}) + \mathrm{O}(\mathrm{Pe}^2)$. It is clear that Pe influences the trajectory of the particle by decreasing its range of motion (that is, the area of the ellipse), particularly in the flow-gradient y direction. This is because of the O(Pe) concentration distribution, which decreases the particle phoretic velocity, thereby restricting the particle to travel a shorter distance before it rotates in the shear flow. Additionally, the trajectory is dependent on the initial orientation of the particle in shear flow. Specifically, the initial orientation determines in which region of the orbit the effect of advection is most prominently felt. For a particle initially aligned with the flow direction, $\psi_0 = 0$, the top of its orbit is displaced at finite Pe. For an initial alignment along the flow-gradient direction, $\psi_0 = \pi/2$, the bottom of the orbit is displaced at finite Pe.

V. CONCLUSIONS

We have investigated the role of ambient fluid flows on the dynamics of an active self-diffusiophoretic colloid. Specifically, our calculations focused on a model spherical Janus particle with a continuous variation in surface activity for solute generation or consumption, placed in a steady simple shear flow. The flow can distort the self-generated solute concentration gradient through advection: the extent of distortion is characterized by a Peclet number, Pe. We computed the distorted concentration and the resulting impact on the particle motion at small Pe using matched asymptotic expansions. Advection of the solute fundamentally alters the particle dynamics: for example, there is an O(Pe) cross-streamline migration and an O($\mathrm{Pe}^{3/2}$) reduction in the velocity

of the particle along its symmetry axis. While our calculations have employed a simple model for surface activity, it is expected that the general conclusions, e.g., O(Pe) cross-streamline migration, hold for more complicated, or realistic, surface reaction distributions and kinetics. The predicted cross-streamline migration is relevant to the purported application of self-propelled particles in blood vessels or microfluidic channels, as it suggests that a suspension of such particles would attain a nonuniform concentration distribution along the cross section of a channel. We have also shown that the planar trajectory of a self-diffusiophoretic particle in shear flow is of elliptical shape, and that the area of the ellipse contracts with increasing Pe. The observation of such an elliptical orbit, whose area decreases with increasing Pe, would provide an experimental test of our calculations. In this regard, recall that an inert particle would simply rotate with angular velocity of the ambient shear without traversing fluid streamlines. Verification of our findings could also come from comparison to molecular simulations: for example, Sharifi-Mood *et al.* [34] recently performed molecular-dynamics simulations of diffusiophoresis in an external solute gradient that showed good agreement with continuum-level calculations.

We have considered only two-dimensional dynamics, wherein the direction of self-propulsion is in the plane of shear. It would be interesting to quantify the particle motion in three dimensions: for example, it is expected on symmetry grounds that a particle translating in a direction orthogonal to the shear flow would experience an $O(Pe^{3/2})$ modification in its velocity of self-propulsion due to solute advection. One could also consider particle motion in two-dimensional mixed linear flows, ranging from pure rotation to planar extension. A further extension of our work is to consider self-diffusiophoresis in Poiseuille flow; here, the varying velocity gradient of the ambient flow would lead to a particle trajectory that is more complicated than the elliptical orbit found in simple shear. A complete analysis of this problem (and also that of self-diffusiophoresis in a Couette flow) must also account for interactions between the Janus particle and the confining boundaries: both solvent-mediated hydrodynamic interactions between the particle and the boundaries, and the effect of the boundaries on the solute concentration distribution. An important question is whether the particle is driven to the center of the flow, to the walls, or attains an intermediate equilibrium position.

Finally, we have neglected the influence of Brownian motion on the particle dynamics, which is a reasonable assumption for relatively large colloids (typically greater than a few microns in diameter). Nonetheless, consideration of the impact of Brownian motion is an interesting question. Recently, Sandoval *et al.* [23] derived (integral) expressions for the mean-square displacement (MSD) tensor of an active particle undergoing time-dependent self-propulsion in a steady two-dimensional linear flow. (They explicitly evaluated the MSD tensor for an active colloid undergoing steady self-propulsion, demonstrating that the MSD thereof can be much greater than an inert particle.) A three-dimensional extension of our calculations would provide the necessary expressions for the time-dependent phoretic particle velocity at small Pe, which could be used in the formalism of Sandoval *et al.* [23] to quantify the impact of Brownian motion on self-diffusiophoresis in a linear flow. We leave this task to future work.

APPENDIX

We write Eq. (22) as $\bar{C}_0^* = 2A(\bar{C}_{0,x}^* + \bar{C}_{0,y}^*)$, where [2]

$$\bar{C}_{0,x}^* = 2A\cos\psi \int_0^\infty \frac{\partial}{\partial \hat{x}} \left\{ \frac{1}{S^{3/2}\left(1+\frac{1}{12}S^2\right)^{1/2}} \times \exp\left[-\left(\frac{\left(\hat{x} - \frac{1}{2}\hat{y}S\right)^2}{4S\left(1+\frac{1}{12}S^2\right)} + \frac{\hat{y}^2+\hat{z}^2}{4S} \right) \right] \right\} dS, \tag{A1}$$

which can be written in spherical coordinates as

$$\bar{C}_{0,x}^* = -A\cos\psi \int_0^\infty \frac{\bar{\rho}\sin\theta\left(\cos\phi - \frac{1}{2}\sin\phi S\right)}{S^{5/2}\left(1+\frac{1}{12}S^2\right)^{3/2}} \times \exp\left[-\bar{\rho}^2 \left(\frac{1+aS+bS^2}{4S\left(1+\frac{1}{12}S^2\right)} \right) \right] dS, \tag{A2}$$

where

$$a = -\tfrac{1}{2}\sin^2\theta\sin\phi\cos\phi, \tag{A3}$$

$$b = \tfrac{1}{3}\sin^2\theta\sin^2\phi + \tfrac{1}{12}\cos^2\theta. \tag{A4}$$

We seek the limit of (A2) as $\bar{\rho} \to 0$. The integral can be split into two regions: an inner region $S \sim O(\bar{\rho}^2)$ and an outer region $S \sim O(1)$. In the inner region, we let $S = \bar{\rho}^2 u$, with $u \sim O(1)$ as $\bar{\rho} \to 0$. We mark the boundary between the two regions as δ, where $\bar{\rho}^2 \ll \delta \ll 1$; thus,

$$\begin{aligned} \bar{C}_{0,x}^* = -A\cos\psi \Bigg\{ & \int_0^{\delta/\bar{\rho}^2} \frac{du\ \bar{\rho}\sin\theta\left(\cos\phi - \frac{1}{2}\sin\phi\bar{\rho}^2 u\right)}{\bar{\rho}^5 u^{5/2}\left(1+\frac{\bar{\rho}^4}{12}u^2\right)^{3/2}} \\ & \times \exp\left[-\left(\frac{1+au+bu^2}{4u\left(1+\frac{\bar{\rho}^4}{12}u^2\right)} \right) \right] \\ & + \int_\delta^\infty \frac{dS\ \bar{\rho}\sin\theta\left(\cos\phi - \frac{1}{2}\sin\phi S\right)}{S^{5/2}\left(1+\frac{1}{12}S^2\right)^{3/2}} \\ & \times \exp\left[-\bar{\rho}^2 \left(\frac{1+aS+bS^2}{4S\left(1+\frac{1}{12}S^2\right)} \right) \right] \Bigg\}. \end{aligned} \tag{A5}$$

In the limit $\bar{\rho} \to 0$, the first (inner) integral in (A5) equals

$$-A\cos\psi\sin\theta\left(-\sqrt{\pi}\frac{(a\bar{\rho}^2 - 4)}{\bar{\rho}^2}\cos\phi - \sqrt{\pi}\sin\phi + \frac{\bar{\rho}\sin\phi}{\delta^{1/2}} - \frac{\bar{\rho}\cos\phi}{\delta^{3/2}} \right) + \cdots, \tag{A6}$$

which can be rewritten as

$$-A\cos\psi\sin\theta\left(-\sqrt{\pi}\sin\phi-\frac{a\bar{\rho}^2-4}{\bar{\rho}^2}\sqrt{\pi}\cos\phi+\int_\delta^\infty\frac{\bar{\rho}\left(-\cos\phi+\frac{1}{2}S\sin\phi\right)}{2S^{5/2}}dS\right)+\cdots. \tag{A7}$$

The leading contribution of the second (outer) integral in (A5) is found by setting $\bar{\rho}=0$ in the exponential term of the integrand. Applying this simplification and substituting (A7) into (A5) yields

$$\bar{C}^*_{0,x}=-A\cos\psi\sin\theta\left\{-\sqrt{\pi}\sin\phi-\frac{a\bar{\rho}^2-4}{\bar{\rho}^2}\sqrt{\pi}\cos\phi+\int_\delta^\infty dS\left(\frac{\bar{\rho}\left(-\cos\phi+\frac{1}{2}S\sin\phi\right)}{2S^{5/2}}+\frac{\bar{\rho}\left(\cos\phi-\frac{1}{2}\sin\phi S\right)}{S^{5/2}\left(1+\frac{1}{12}S^2\right)^{3/2}}\right)\right\}. \tag{A8}$$

At the present order of approximation, the lower limit of the integral in the above can be taken as zero, yielding

$$\bar{C}^*_{0,x}=-A\cos\psi\sin\theta\left\{-\sqrt{\pi}\sin\phi-\frac{a\bar{\rho}^2-4}{\bar{\rho}^2}\sqrt{\pi}\cos\phi+\bar{\rho}\int_0^\infty\left(\frac{\left(\cos\phi-\frac{1}{2}S\sin\phi\right)\left[1-\left(1+\frac{1}{12}S^2\right)^{3/2}\right]}{S^{5/2}\left(1+\frac{1}{12}S^2\right)^{3/2}}\right)dS\right\}. \tag{A9}$$

Upon numerical evaluation of the integral, we find

$$\bar{C}^*_{0,x}=-A\cos\psi\left(\frac{4\sqrt{\pi}}{\bar{\rho}^2}\sin\theta\cos\phi+\frac{\sqrt{\pi}}{2}\sin^3\theta\sin\phi\cos^2\phi-\sqrt{\pi}\sin\theta\sin\phi-0.479\bar{\rho}\sin\theta\cos\phi+0.683\bar{\rho}\sin\theta\sin\phi\right), \tag{A10}$$

with numerical coefficients reported to three decimal places. This can be written in Cartesian coordinates as

$$\bar{C}^*_{0,x}=-A\cos\psi\left(\frac{4\sqrt{\pi}}{\bar{\rho}^3}\hat{x}+\frac{\sqrt{\pi}}{2\bar{\rho}^3}\hat{x}^2\hat{y}-\frac{\sqrt{\pi}}{\bar{\rho}}\hat{y}-0.479\hat{x}+0.683\hat{y}\right). \tag{A11}$$

Following a similar method, $\bar{C}^*_{0,y}$ is found to be

$$\bar{C}^*_{0,y}=\frac{A}{2}\sin\psi\left\{2\sqrt{\pi}\frac{\hat{x}}{\bar{\rho}}-\sqrt{\pi}\frac{\hat{x}\hat{y}^2}{\bar{\rho}^3}+4\sqrt{\pi}\frac{\hat{x}}{\bar{\rho}^3}-1.342\hat{y}-1.366\hat{x}\right\}. \tag{A12}$$

Combining (A11) and (A12) yields

$$\begin{aligned}\bar{C}^*_0=A\Bigg[&\cos\psi\left(0.479\hat{x}-0.683\hat{y}-\frac{4\sqrt{\pi}}{\bar{\rho}^2}\hat{x}-\frac{\sqrt{\pi}}{2\bar{\rho}^3}\hat{x}^2\hat{y}+\frac{\sqrt{\pi}}{\bar{\rho}}\hat{y}\right)\\&+\sin\psi\left(-0.683\hat{x}-0.671\hat{y}+\frac{2\sqrt{\pi}}{\bar{\rho}^3}\hat{x}-\frac{\sqrt{\pi}}{2\bar{\rho}^3}\hat{x}\hat{y}^2+\frac{\sqrt{\pi}}{\bar{\rho}}\hat{x}\right)\Bigg].\end{aligned} \tag{A13}$$

Returning to spherical coordinates delivers Eq. (23) in the main text.

[1] J. L. Anderson, Annu. Rev. Fluid Mech. **21**, 61 (1989).
[2] L. G. Leal, Chem. Eng. Commun. **1**, 21 (1973).
[3] A. Erbe *et al.*, J. Phys.: Condens. Matter **20**, 404215 (2008).
[4] S. J. Ebbens and J. R. Howse, Soft Matter **6**, 726 (2010).
[5] W. F. Paxton, P. T. Baker, T. R. Kline, Y. Wang, T. E. Mallouk, and A. Sen, J. Am. Chem. Soc. **128**, 14881 (2006).
[6] N. Sharifi-Mood, J. Koplik, and C. Maldarelli, Phys. Fluids **25**, 012001 (2013).
[7] X. Zheng, B. ten Hagen, A. Kaiser, M. Wu, H. Cui, Z. Silber-Li, and H. Löwen, Phys. Rev. E **88**, 032304 (2013).
[8] I. Buttinoni, J. Bialké, F. Kümmel, H. Löwen, C. Bechinger, and T. Speck, Phys. Rev. Lett. **110**, 238301 (2013).
[9] F. Kümmel, B. ten Hagen, R. Wittkowski, I. Buttinoni, R. Eichhorn, G. Volpe, H. Löwen, and C. Bechinger, Phys. Rev. Lett. **110**, 198302 (2013).
[10] W. F. Paxton *et al.*, J. Am. Chem. Soc. **126**, 13424 (2004).
[11] J. R. Howse, R. A. L. Jones, A. J. Ryan, T. Gough, R. Vafabakhsh, and R. Golestanian, Phys. Rev. Lett. **99**, 048102 (2007).
[12] R. Golestanian, T. B. Liverpool, and A. Ajdari, New J. Phys. **9**, 126 (2007).
[13] Y. Tao and R. Kapral, Soft Matter **6**, 756 (2010).
[14] M. E. Cates, S. M. Fielding, D. Marenduzzo, E. Orlandini, and J. M. Yeomans, Phys. Rev. Lett. **101**, 068102 (2008).
[15] B. ten Hagen, R. Wittkowski, and H. Löwen, Phys. Rev. E **84**, 031105 (2011).
[16] S. Muhuri, M. Rao, and S. Ramaswamy, Europhys. Lett. **78**, 48002 (2007).
[17] M. Tarama, A. M. Menzel, B. ten Hagen, R. Wittkowski, T. Ohta, and H. Löwen, J. Chem. Phys. **139**, 104906 (2013).
[18] G. P. Saracco, G. Gonnella, D. Marenduzzo, and E. Orlandini, Cent. Eur. J. Phys. **10**, 1109 (2012).
[19] A. Zöttl and H. Stark, Phys. Rev. Lett. **108**, 218104 (2012).

[20] Figure 2-325. R. H. Perry and D. W. Green, *Perry's Chemical Engineers' Handbook*, 8th ed. (McGraw-Hill, New York, 2008).
[21] A. S. Khair, J. Fluid Mech. **731**, 64 (2013).
[22] S. Michelin and E. Lauga, J. Fluid Mech. **747**, 572 (2014).
[23] M. Sandoval, N. K. Marath, G. Subramanian, and E. Lauga, J. Fluid Mech. **742**, 50 (2014).
[24] W. F. Paxton, S. Sundararajan, T. E. Mallouk, and A. Sen, Angew. Chem. Int. Ed. Engl. **45**, 5420 (2006).
[25] J. Wang and W. Gao, ACS Nano **6**, 5745 (2012).
[26] T. J. Pedley, *The Fluid Mechanics of Large Blood Vessels* (Cambridge University Press, Cambridge, 1980).
[27] H. H. Lipowsky, S. Kovalcheck, and B. W. Zweifach, Circ. Res. **43**, 738 (1978).
[28] R. Kapral, J. Chem. Phys. **138**, 020901 (2013).
[29] K. V. Sharp, R. J. Adrian, J. G. Santiago, and J. I. Molho, *Liquid Flows in Microchannels*, *The MEMS Handbook*, 2nd ed. (CRC, Boca Raton, FL, 2005).
[30] J. L. Anderson, D. C. Prieve, and J. P. Ebel, Chem. Eng. Commun. **55**, 211 (1987).
[31] J. L. Anderson and D. C. Prieve, Langmuir **7**, 403 (1991).
[32] N. Frankel and A. Acrivos, Phys. Fluids **11**, 1913 (1968).
[33] D. E. Elrick, Aust. J. Phys. **15**, 283 (1962).
[34] N. Sharifi-Mood, J. Koplik, and C. Maldarelli, Phys. Rev. Lett. **111**, 184501 (2013).